JOURNAL OF
Optical Communications
and Networking

Optical-access networks for smart sustainable cities: from network architecture to fiber deployment

Md Mosaddek Hossain Adib,[1,2,†,*] Patrick Matalla,[1,†] Christoph Füllner,[1,2] Shi Li,[3] Elias Giacoumidis,[3] Christian Raack,[4] Ulrich Menne,[4] Michael Straub,[2] Tarek Saier,[5] Christoph Schweikert,[6] Stefan Orf,[7] Martin Gontscharow,[7] Tobias Käfer,[5] Michael Färber,[5,8] André Richter,[3] René Bonk,[2] and Sebastian Randel[1]

[1]Institute of Photonics & Quantum Electronics, Karlsruhe Institute of Technology, Karlsruhe, Germany
[2]Nokia Bell Labs, Stuttgart, Germany
[3]VPIphotonics GmbH, Berlin, Germany
[4]atesio GmbH, Berlin, Germany
[5]Institute of Applied Informatics & Formal Description Methods, Karlsruhe Institute of Technology, Karlsruhe, Germany
[6]TelemaxX Telekommunikation GmbH, Karlsruhe, Germany
[7]FZI Research Center for Information Technology, Karlsruhe, Germany
[8]Currently at AI Center ScaDS.AI, Technical University Dresden, Dresden, Germany
[†]These authors contributed equally to this work.
[*]md.adib@nokia-bell-labs.com

Received 1 October 2024; revised 24 December 2024; accepted 29 December 2024; published 27 February 2025

With the steadily progressing digitization of our society and the migration into urban areas, digitized and highly connected smart cities have attracted much attention from the research community due to their impact on everyday life, potential for new innovations, and ability to reduce carbon footprints. The versatile applications, which are intended to improve life in cities in various aspects, have one thing in common—they rely on widespread, reliable, and high-performing communication networks. Therefore, optical-access networks will be a crucial part of the smart cities' network infrastructure as they provide cost-effective and high-speed connectivity to antenna sites, residents, enterprises, businesses, and regional data centers in a point-to-multipoint topology. In this article, we address the overall impact of this urban transformation on such networks. We outline our vision of the future smart sustainable city, which will leverage advanced optical-access networks. Subsequently, the physical layer design of optical-access networks is analyzed in the context of point-to-multipoint network topology. This includes a 100-Gbit/s intensity-modulation and direct-detection passive optical network (PON) and a 200-Gbit/s coherent PON utilizing eight-digital subcarrier-based time- and wavelength-division multiplexing and coherent detection. We discuss artificial intelligence-based network monitoring and resource allocation. Next, we provide a techno-economical study for sustainable fiber deployment strategies. Finally, we report the results of a network demonstration for the remote assistance of a connected autonomous vehicle.

https://doi.org/10.1364/JOCN.542368

1. INTRODUCTION

The digitization of societies around the globe continues apace. Omnipresent connectivity in conjunction with artificial intelligence will make it possible to automate and optimize more and more processes in almost all aspects of life. In many areas, the vision of a smart sustainable city in which a large number of people, devices, and machines communicate with each other is starting to become reality. As a result, the International Telecommunication Union (ITU) predicts 97 billion mobile connected devices by 2030, around 14 times more compared to 2020 and more than 10 times the human population [1]. In future cities, this will include a large number of connected self-driving vehicles, which will exchange immense amounts of data with other road users and an intelligent infrastructure, imposing stringent demands on the underlying networking infrastructure. This scenario together with a wide spectrum of novel services and applications will be made possible by the ongoing rollout of the fifth generation (5G) mobile network

and, expected by 2030, the sixth generation (6G) mobile network, which will feature increased data rates and reduced latency by densifying mobile cell sites and by utilizing additional frequency bands [2]. Optical networks, which utilize the vast bandwidth of low-loss optical fibers, are used to aggregate the data traffic of cell sites, homes, enterprises, and sensor nodes in central offices and regional data centers [3,4]. Besides the installation of a mobile network, the smart sustainable city will require the rollout of a next-generation fiber-optic network, which addresses the diverse requirements, e.g., in terms of data rate, latency, security, as well as operational and capital expenditures.

In this article, we describe our vision of a smart sustainable city, from which we derive the requirements for future fiber-optic access networks. Taking a holistic approach, we discuss how passive optical networks (PONs) can be scaled to provide high data rates and low latencies as well as network monitoring and dynamic resource allocation. We further present the results of a techno-economical study for a sustainable fiber rollout in the city of Karlsruhe, a city in Germany with approximately 300,000 residents. In the final section, we report on the access network demonstration of remote assistance for a connected autonomous vehicle. This paper provides an overview of the various results achieved within a three-year joint project named KIGLIS funded by the German Federal Ministry of Education and Research (BMBF). The KIGLIS project can be found here [5].

2. VISION OF A SMART SUSTAINABLE CITY

The smart sustainable city uses advanced technologies to improve the quality of life of its residents, businesses, and visitors, while answering the economic, social, environmental, and cultural needs of current and future generations [6]. In this context, the smart city has to address the challenges and issues residents of modern cities are facing today. One example is the traffic situation, where congested streets and occupied parking spaces lead to carbon emissions, air pollution, stress, and accidents. Another example is the monitoring of environment and infrastructure, e.g., for city-wide waste management, disaster prevention, and safety. It is thereby imperative that all technical solutions comply with the prevailing laws concerning, e.g., privacy, safety, and data protection. In the future smart sustainable city, a variety of connected services in the fields of economy, mobility, living, governing, and social affairs [7] place stringent demands on the underlying communication infrastructure in terms of security, latency, speed, management, and energy efficiency.

A key enabler for this is a ubiquitous and seamless communication infrastructure which includes broadband wireless and fiber-optic access, e.g., using Wi-Fi and 5G/6G, sensor networks based on LoRaWAN [8], and regional data centers, allowing high-performance, energy-efficient, and secure processing and storage of data. Our envisioned smart sustainable city is illustrated in Fig. 1. The realization of automated driving in a densely populated city will not only require a large number of sensors such as cameras, radars,

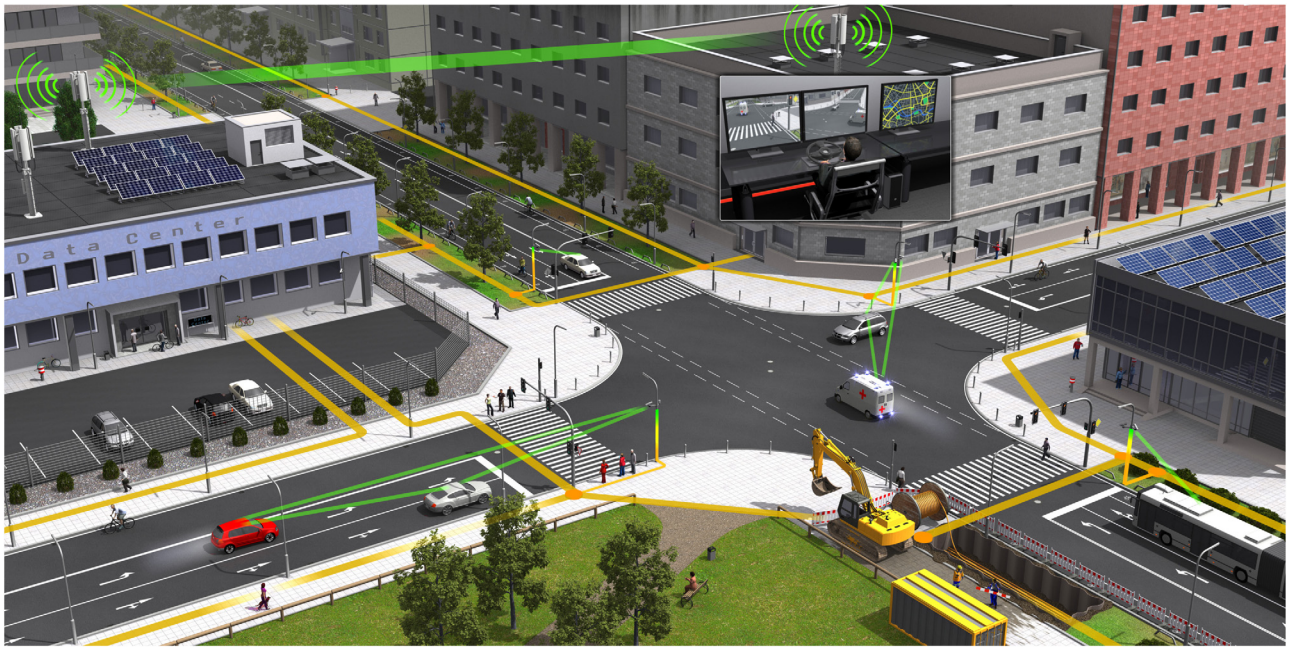

Fig. 1. Vision of a smart sustainable city incorporating a dense fiber-optic network (yellow lines) enabling high-speed wireless connectivity (green lines). Small cells, integrated, e.g., in street and traffic lights, provide low-latency broadband access for diverse applications, such as connected driving, augmented reality, and smart-city monitoring. In addition, high-speed wireless point-to-point links complement the fiber network where fiber deployment is difficult, or as redundant/protection paths. Associated processing and storage needs for smart-city applications and services are accommodated in regional data centers. From an infrastructure control center, a remote operator can provide assistance to autonomous vehicles in critical situations. In this scenario, an ambulance equipped with network connectivity transmits vital information to the smart-city monitoring system and nearby vehicles as it crosses a junction. This is achieved using high-speed wireless, point-to-multipoint optical access, and vehicle-to-vehicle communication technologies.

lidars, and microphones located in cars or at the traffic infrastructure but also a high-speed and low-latency communication infrastructure that allows us to aggregate this data. This makes it possible to create a digital twin of the cities' traffic situation in real time. Artificial intelligence (AI) algorithms can then be used to optimize processes in the city and to enable secure automated driving. In a complex driving situation, a human remote operator can access the data and safely steer the vehicle around an obstacle. Processing and storing the data in regional data centers is not only energy-efficient but also allows privacy and data security.

In order to facilitate such a scenario, we envision a dense fiber-optic network based on optimized PON not only households and enterprises but also wireless small cells with high bandwidth and low latency to data centers within distances of up to 20 km [9,10]. This allows us to find locations also outside the expensive city centers. In the following, we look at various aspects of optical-access networks on different layers: network architecture, network maintenance, resource allocation, and, finally, aspects of sustainable fiber rollout.

3. FIBER-OPTIC NETWORK TECHNOLOGIES

This section covers the aspects of a smart-city PON on the physical layer. Section 3.A provides an overview of recent advances in PON standardization and the working principle of a PON system, followed by the requirements of our envisioned smart-city PON architecture. In Sections 3.B and 3.C, we then present our research results for a 100-Gbit/s intensity-modulation and direct-detection (IM/DD) and a 200-Gbit/s coherent high-speed PON, respectively. Finally, in Section 3.D, we investigate machine learning methods to monitor the PON infrastructure more efficiently and possibly predict failures.

A. Passive Optical Networks

PONs represent the preferred network architecture in fiber-optic access. As a point-to-multipoint network based on bidirectional transmission over a single fiber and a purely passive optical splitter, they require significantly fewer active devices when compared to a point-to-point network. The most frequently deployed PON standards are the gigabit PON (GPON) and its successor, the symmetric 10-Gbit/s PON (XGS-PON). The highest capacity commercially available today is offered by the symmetric 25-Gbit/s PON that is defined in a multi-source agreement (25GS-PON MSA) [11,12]. Recently, a 50-Gbit/s PON standard was agreed upon and is expected in the market a few years from now [13]. In all these standards, the intensity of the light emitted by a laser is modulated by data and a single photodiode converts the received optical power into an electrical current—a scheme commonly referred to as intensity modulation and direct detection (IM/DD). In the optical distribution network (ODN), connecting a central office to a number of 32 or 64 endpoints over distances up to 20 km, a common feeder fiber is split using an optical power splitter. The total loss in the splitter, the fiber, splices, connectors together with a network deployment margin can be as high as 28 dB or even 35 dB according to the budget classes of the PON standards mentioned above, e.g., the 50G-PON [13]. The specified receiver sensitivity dictates the transmitted optical power that also has to take the optical path penalty, introduced, e.g., by chromatic dispersion (CD) and fiber nonlinearities, into account. In downstream, the optical line termination (OLT) sends a continuous stream of data that is distributed to all optical network units (ONUs), which select only the allocated grants for further processing. In the upstream direction, the OLT is dynamically allocating time slots, in which the ONUs are allowed to transmit. This way, the PON is a shared medium using time-division multiplexing (TDM) in downstream and time-division multiple access (TDMA) in upstream.

We envision that an evolved PON standard, which will likely be standardized in the time frame from 2025 to 2030, will further extend the possibilities of today's PON generations towards the requirements of future smart sustainable cities, such as new bandwidth-hungry services and a massive number of connected sensors. The large variety of smart-city services will impose high demands in terms of data rate, reliability, latency, cost, flexibility, and energy efficiency [14]. Currently, it is an open question whether a 100-Gbit/s or a 200-Gbit/s PON should follow the 50-Gbit/s PON. Since 25G-PON, the PON transceiver technology is following the data center market trends [15]. Therefore, the best course for PON is to focus on the same 2× increase in symbol rate as the ecosystem that it is leveraging. Thus, we focus our investigations on a future 100-Gbit/s IM/DD-PON and 200-Gbit/s coherent subcarrier PON for our smart-city concept. Considering the demands for high bandwidth and low latency, we expect that the future PON will have to offer not only a data rate of 100 Gbit/s or more, but also a latency of below 1 ms and 99.999% reliability. We present our results from the KIGLIS project considering two different 100-GBd-capable PON architectures.

B. IM/DD 100 Gbit/s PON

All PON standards mentioned above employ non-return-to-zero (NRZ) on-off keying (OOK) as the modulation format. So far, this format has prevailed because of its simplicity, its high tolerance against device nonlinearities, and its high receiver sensitivity. However, scaling to data rates of 100 Gbit/s and above will significantly reduce the tolerance versus CD, which is inversely proportional to the square of the symbol rate. Furthermore, bandwidth limitations of low-cost components will impair the signal quality. These drawbacks can be mitigated by increasing the spectral efficiency using a higher-order modulation format, e.g., quaternary pulse-amplitude modulation (4-PAM), in combination with adaptive equalization and forward-error correction (FEC) [16]. However, realizing a loss budget of around 30 dB poses a challenge, as 4-PAM modulation requires a significantly higher signal-to-noise ratio in comparison to OOK [17].

Figure 2 depicts our envisioned link configuration for the downstream of a 100-Gbit/s IM/DD PON using 4-PAM modulation. At the transmitter, we consider a distributed-feedback (DFB) laser emitting in O-band at a wavelength around 1344 nm in order to study the CD tolerance. The O-band has the benefit that the CD is significantly lower

than in C-band around 1550 nm; however, this comes at the cost of a slightly increased fiber loss. We consider an electro-absorption modulator (EAM) [18], whose nonlinearity is pre-compensated using digital signal processing (DSP). At the receiver side, an avalanche photodiode (APD) followed by a transimpedance amplifier (TIA) is used to convert the received optical signal into an electrical one. APDs are commonly used in PONs, since they offer a higher receiver sensitivity compared to PIN photodiodes, which allow achieving high loss budgets. Finally, the received signal is processed using DSP. We simulate the proposed 100-Gbit/s 4-PAM downstream link as shown in Fig. 2 in a numerical simulation using the commercial software *VPItransmissionMaker Optical Systems* [19]. In O-band (1344 nm), we explore the effect of using an EAM with certain chirp characteristics. The bandwidth of the EAM is set to 55 GHz, and electrical noise is set to 20 pA/Hz$^{1/2}$. We found best performance for a drive signal with peak-to-peak voltage of 1.6 V and a EAM bias of −90 V. The inset in Fig. 3 shows the transfer function of the EAM and its measured chirp. To reduce the system costs, we excluded RF driver amplifiers, and the optical launch power is set to 8.8 dBm. For the standard single-mode fiber, we used a CD coefficient of 3.85 ps/nm/km, a CD slope of 0.092 ps/(km × nm^2), an attenuation of 0.35 × 10^{-3} dB/km, and a nonlinearity index of 2.6 × 10^{-20} m^2/W. At the receiver, we consider an APD/TIA with a bandwidth of only 25 GHz, which would allow the reuse of low-cost components from 50G-PON ONUs. The electrical low pass filters at both the OLT and ONU were of fourth-order Bessel type. At the OLT transmitter, we performed an optimization of the PAM4 symbol levels. At the ONU, the receiver DSP includes timing synchronization, a five-tap data-aided feedforward equalizer, and FEC with 15% overhead and a bit-error ratio (BER) threshold of 0.0125 [20]. In Fig. 3, we compare the receiver sensitivity for optical back-to-back and for 20 km fiber either without or with chirp of the EAM. We find that CD leads to a 1-dB sensitivity penalty if no chirp is considered. With the chirp, this penalty increases to 2 dB. For the latter case, a receiver sensitivity of −22 dBm is achieved, which results in a total link budget of 30.8 dB. Therefore, the simulation shows that the proposed IM/DD PON can indeed fulfill the data-rate and link-budget requirements of a PON serving a future smart sustainable city. Further receiver sensitivity improvements can be achieved by replacing the linear five-tap equalizer by neural-network-based equalizers. As discussed in [21–24], these allow the compensation of nonlinear effects caused, for example, by the EAM, gain saturation of semiconductor optical amplifiers (SOAs), or increased chromatic dispersion in C-band PONs at the expense of increased computational complexity.

With the rising number of digital services in a smart sustainable city, the number of optical network users may grow up to 256 users in the future [25]. Increasing the split ratio from 64 to 256 results in a reduction in optical power of around 6 dB per ONU branch. In order to maintain PON fiber distances of up to 20 km, a larger loss budget is therefore required, e.g., through the use of optical amplifiers. In addition, a larger number of network subscribers has an influence on the burst duration. In order to guarantee the same latency as for 64 users, the burst duration must be shortened. Each burst consists of a

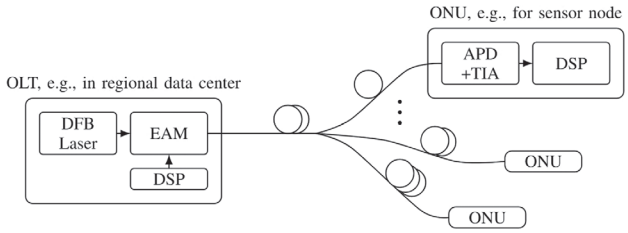

Fig. 2. Downstream link configuration of the envisioned 100-Gbit/s IM/DD PON.

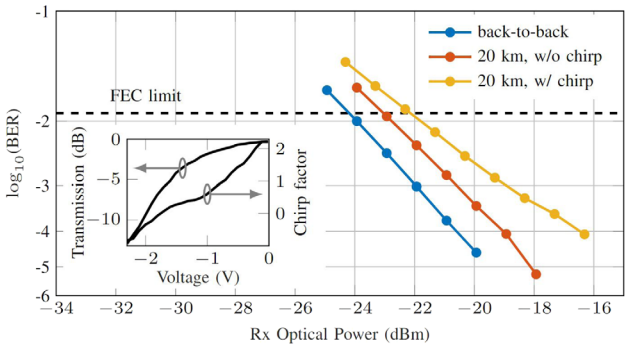

Fig. 3. Simulation results for IM/DD PON downstream operation. The inset shows the transmission and chirp characteristics of the EAM.

preamble for identification and synchronization of the signal as well as the data. Shortening the burst duration while maintaining the same preamble length therefore results in a reduced data throughput. Consequently, in future high-speed PONs, the question arises as to what extent the preamble can be shortened using blind and digital synchronization procedures. A digital clock synchronization can be implemented either in a feedback architecture based on a phase-locked loop (PLL) or in a fully digital feedforward architecture. Due to the relatively long acquisition time of the PLL, the latter may not meet the stringent requirements of fast synchronization in burst-switched systems. In contrast to that, feedforward clock recoveries offer instantaneous timing estimation and improved high-frequency jitter performance, especially when using low-cost oscillators. In [26,27], we analyze a digital feedforward clock recovery and compare it to a digital feedback clock recovery in a 112-Gbit/s PON upstream in C-band using two bursts. Figure 4 shows the experimental results obtained for the clock synchronization for alternating 4.5812-µs-long silent 2-PAM and loud 4-PAM bursts with a burst pause of 0.2 µs and free-running transmitter and receiver oscillators with a nominal clock frequency offset of 1 ppm. It can be seen that instantaneous timing acquisition is achieved when using a feedforward clock recovery, which enables synchronization within nanoseconds. In this particular example, we used an additional moving average filter for the estimation, which leads to a total synchronization time of 36.57 ns. In contrast to that, the feedback loop converges more slowly for low SNR and stable synchronization starts at the end of the burst. Here, an ideal feedback-loop latency of one clock cycle was simulated. However, in reality, the loop latency can amount to tens to hundreds of clock cycles, which significantly deteriorates the stability and convergence speed

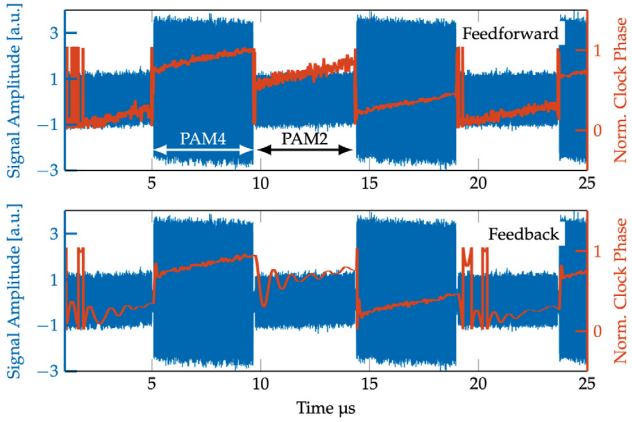

Fig. 4. Received AC-coupled burst-mode signal after resampling in a 56 GBd IM/DD PON upstream using free-running transmitter and receiver oscillators with a nominal clock frequency offset of 1 ppm and estimated sampling offset for a representative feedback and feedforward clock recovery algorithm over time.

of the control loop [27]. For this reason, digital feedforward clock synchronization is a promising method to replace bulky analog clock and data recovery circuits in current PONs by energy-efficient, compact, and ultra-fast digital circuits, which furthermore allow a reduction of the preamble length.

C. 200 Gbit/s Coherent Subcarrier PON

In metro- and long-haul optical networks as well as data center interconnects, coherent systems have replaced IM/DD systems since they allow increased spectral efficiency by exploiting quadrature and polarization multiplexing of the complex optical field as well as electronic CD compensation using linear filters implemented in DSP. The latter allows us to operate the PON outside the occupied O-band frequencies, e.g., in C-band. Furthermore, coherent receivers provide a higher receiver sensitivity [28]. Within the past 15 years, digital coherent transceiver technology has matured significantly in terms of footprint, power consumption, and cost. This poses the question of whether coherent transceivers have the potential to replace IM/DD also in optical-access networks. However, the complexity of coherent transceivers remains significantly higher compared to their IM/DD counterparts. Despite that, the introduction of coherent transceivers could be a potential solution for very high-speed PONs (VHSPs), as they provide high sensitivity, flexibility, and a pay-as-you-grow model. The adoption of coherent technology in PONs is driven by its widespread use in the data center market and research breakthroughs that could lead to a further reduction in their cost structures [15,29]. In recent years, several coherent PON architectures based on simplified and full coherent receivers have already been proposed [30–34], such as coherent ultra-dense (UD) wavelength-division multiplexing (WDM) PONs in [31], a digital subcarrier based PTMP network in [32], and rate-flexible time-and-frequency division multiplexing (TFDM) PONs in [33]. Note that, e.g., the simplified coherent receiver based on Alamouti coding represents a trade-off between bandwidth requirements and optical front-end complexity [34].

The requirement for an external cavity laser (ECL) with wavelength tunability, which serves as a local oscillator (LO) at the ONU receiver, is one of the major cost drivers that needs to be avoided. In the KIGLIS project, we explore the scalable coherent PON architecture based on time, wavelength, and subcarrier division multiplexing. The conceptual system diagram is illustrated in Fig. 5(a). Note that it is of upmost importance to keep the complexity and cost of the ONU transceivers as low as possible due to the cost restriction. As mentioned above, coherent transceivers typically use ECLs with wavelength locker and temperature control. In the ONUs of coherent PONs, such frequency stabilized narrow linewidth lasers are prohibited due to their complexity and cost [35]. In the ONU, we therefore share a single DFB laser as a LO and as a transmit laser. Typically, ONUs must support a wide temperature range from -40°C to $+80$°C, while the emission wavelength of DFB lasers shifts by about 0.12 nm/°C, resulting in a frequency range of 1.8 THz [35,36]. Using a simple heater or thermo-electric cooler (TEC), it becomes possible to tune the temperature by a few tens of degrees, resulting in a residual frequency range Δf_{tune} of, e.g., 300 GHz. This leads to a wavelength alignment issue for coherent PONs. In [37], we showed that this issue can be overcome by using a frequency comb source in the OLT. As shown in Fig. 5 inset Ⓐ, a pair of cyclic arrayed-waveguide gratings (CAWGs) is used in the central office (CO) to divide the comb lines with free-spectral range Δf_{FSR} into multiple interleaved wavelength sets which allow scalable pay-as-you-grow WDM. The frequency comb is shared between downstream and upstream, where it is used as a LO. We consider dual-polarization (DP) inphase/quadrature modulators (IQMs) and coherent receivers (CRXs), which can be integrated in either silicon or indium phosphide (InP) as well as an application-specific integrated circuit (ASIC) for the DSP. In the upstream, the CRX must support burst-mode (BM) operation. In the OLT, we consider an optical booster amplifier as well as an optical pre-amplifier. As an example, the multiplexing of two wavelength sets corresponding to two independent OLTs is illustrated in Fig. 5(b). The DFB-LOs can be thermally tuned to the middle of the closest copy of the subcarriers, shown in gray vertical lines. Moreover, multiple digitally generated subcarriers are multiplexed, allowing the medium access control (MAC) to flexibly map dedicated subcarriers, e.g., for low-latency virtual point-to-point (PTP) traffic on some subcarriers while other subcarriers are shared among multiple ONUs using TDMA. Figure 5(c) shows an example of how the eight subcarriers of OLT_1 can be allocated across a set of ONUs. This scheme also allows us to choose different modulation formats for different sub-carriers based on the channel condition or the capacity-versus-loss-budget trade-off [38–40]. We set up a proof-of-concept experiment to validate the scalable coherent PON architecture [37,41,42]. In the experiment, we employ a mode-locked-laser diode (MLLD) with $\Delta f_{\text{FSR}} = 50$ GHz as the frequency comb source, whose optical spectrum is shown in Fig. 5(a) inset ①. Using a programmable optical filter (POF) we select multiple comb lines to emulate wavelength multiplexing of two OLTs. In the digital domain, we create eight subcarriers on a 3.4375 GHz grid and modulate them with random differentially encoded QPSK symbols at 3.125 GBd. The optical

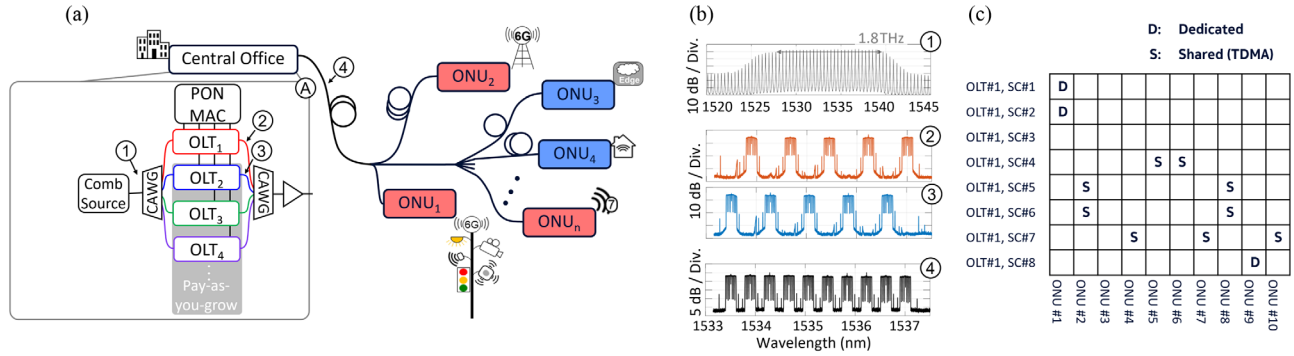

Fig. 5. Scalable coherent PON. (a) Proposed architecture based on digital subcarrier multiplexing and wavelength-division multiplexing addressing the needs of diverse smart-city services. The inset Ⓐ shows the detailed structure of the central office. (b) Optical spectra measured at various positions in the network as indicated by ①, ②, ③, and ④ in (a). (c) Example of digital subcarrier allocation for OLT1 to different ONUs.

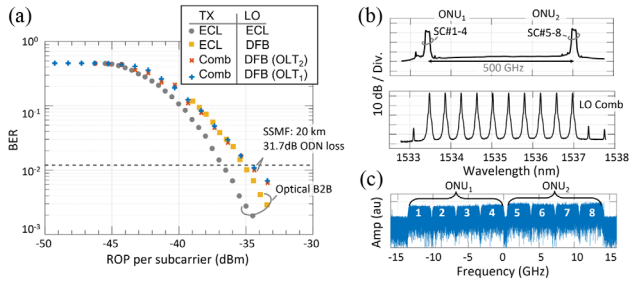

Fig. 6. Experimental results for a coherent PON. (a) Measured downstream BER as a function of the average ROP per subcarrier averaged over all eight subcarriers for different combinations of transmit and LO lasers. (b) Top: measured optical spectrum at the OLT for upstream with two ONUs having a frequency spacing of 500 GHz. Bottom: optical spectrum of the filtered frequency comb used as a LO in the OLT. (c) Electrical spectrum of the received upstream signal including subcarriers from both ONUs.

spectra of the emulated wavelength channels corresponding to OLT_1 and OLT_2 as well as the combined spectrum are shown in Fig. 5(b) insets ②–④. Figure 6 shows our experimental results for downstream. As a reference, we employ an ECL at 1535.5 nm as a transmit laser at the OLT side and a second ECL as a LO at the ONU side. The BERs as a function of the average received optical power (ROP) per subcarrier are shown in Fig. 6(a). We observe a receiver sensitivity of −36.7 dBm per subcarrier. Next, we replace the ECL by a DFB laser as a LO and we observe 1.5 dB penalty, due to increased phase noise. In a next step, we replace the ECL transmitter by the amplified and filtered MLLD and emulate two wavelength-multiplexed OLTs with five signal copies each. In that experiment, we investigate the performance with 20 km standard single-mode fiber (SSMF) and a total ODN loss of 31.7 dB. We observe no additional penalty. Considering a total launch power of 16 dBm and a FEC limit of 0.0125 [20], downstream operation at an aggregate bit rate of 200 Gbit/s is successfully demonstrated. For upstream, we emulate two ONUs each modulating four subcarriers using two DFB lasers emitting at frequencies about 500 GHz apart. The resulting upstream spectrum is shown in Fig. 6(b) together with the 10 comb lines used as a LO. The corresponding electrical spectrum is shown in Fig. 6(c).

In summary, we proposed and experimentally demonstrated a novel 200-Gbit/s scalable coherent PON architecture based on digital subcarrier and wavelength-division multiplexing. The architecture addresses the wavelength matching challenge of coherent PONs by using a comb source in the OLT. This allows the use of low-cost DFB lasers in the ONUs. Furthermore, this architecture allows flexible bandwidth allocation, also offering virtual point-to-point and point-to-multipoint connectivity for converged services over the same ODN. Wavelength-division multiplexing along with time-division and subcarrier multiplexing allows pay-as-you-grow and a boost of the ODN capacity towards Tbit/s, while still allowing for coexistence with legacy PON generations (e.g., GPON, XGS-PON, 25G, and 50G PON).

D. Dense Network Monitoring

With increasing connectivity in smart cities, the fiber-optic network is expanding as well. This requires PONs with up to 256 network users [25]. Monitoring and maintaining such large networks is a challenge for network providers. We envision that future sustainable smart cities will employ AI-based PON/ODN monitoring. Figure 7(a) shows one possible AI implementation, where different types of current data [such as optical time-domain reflectometer (OTDR) traces, transmission convergence (TC) layer data, and physical (PHY) layer data] and historical data (such as event simulation, network simulation, deployment data, historic OTDR traces, TC layer data, PHY layer data, etc.) are used. It will employ a sense, think, and act methodology. Currently, OTDRs are often used by network operators for fiber diagnostics and trouble-shooting. Such devices emit short laser pulses into the fiber and then detect the power of back-scattered and back-reflected light. With knowledge about the deployed fiber type, a measurement of the associated time of flight can be used to generate a trace profile of the fiber. This trace comprises distinct peaks resulting from strong back-reflections at splitters, connectors, fiber breaks, and fiber endpoints; see Fig. 7(b). By comparing OTDR scans at different times, fiber breaks can be detected as suddenly appearing anomalies. However, straight identification of failures in the fibers connecting the ONUs to the feeder fiber (drops) is difficult to locate since light is

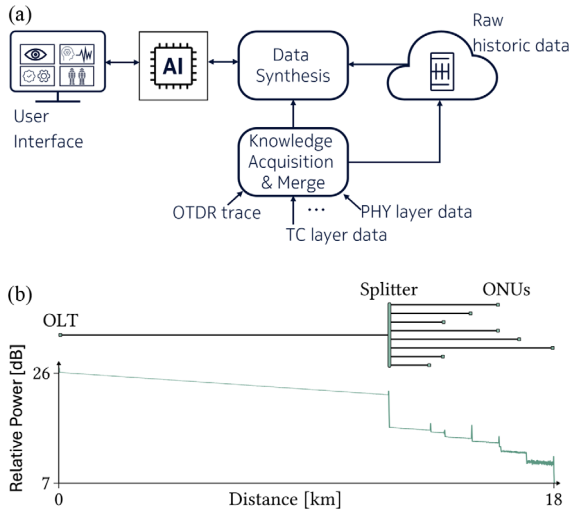

Fig. 7. Dense network monitoring. (a) Concept for AI-based PON/ODN monitoring. (b) Example of an ODN with corresponding OTDR trace.

reflected from all drops to the OLT simultaneously. Typically, this issue is cleared up by affected customers reporting a loss of Internet connection via another intact communication channel. However, such customer feedback will be lacking as soon as machines are connected to the ONU and no human users are present. A second challenge is given by the fact that OTDR measurements only detect existing fiber damages but do not provide any means for failure prediction and prevention. Machine learning (ML) algorithms are predestined to address both of these challenges. In order to determine the exact location of fiber damage behind a passive splitter, ML algorithms consider OTDR traces as well as network deployment data (e.g., fiber lengths, splitting ratio, and component location) to make predictions on which OTDR events originate from which drop. Towards this goal, we investigate the task of OTDR event classification, i.e., assigning an event class (reflection, attenuation, or no event) to each of the discrete time steps in an OTDR trace. We compare the performance of an ML model against a simple heuristic baseline. Our baseline model predicts events based on a set of heuristic rules defined on the rate of change in the OTDR trace's power level. For our ML model we use a random forest [43], a model that learns and averages over multiple classifiers to improve stability. We use an ensemble of 50 classifiers, which, like the baseline, takes the rate of change in power level as input. Evaluating both models on 180 OTDR traces from a 1:8 point-to-multipoint PON, we measure precision and recall scores (reported as the macro average over all classes) of 52% and 69% for the baseline and 98% and 95% for the ML model. For the ML model this tells us that, averaged over all three classes, in 98% the predicted class assignment is correct, and 95% of all time steps per event class are retrieved correctly. In [44], we report the detail about the ML approaches for OTDR diagnoses in PON. To enable permanent monitoring of the fiber-optic network with network anomalies forecasting, neural networks can be trained on large quantities of historical records comprising time series of OTDR measurements and associated network faults. By training on such data, predictions can be made to forecast future network faults and intervene before they occur.

4. NETWORK RESOURCE ALLOCATION

High quality of experience (QoE) is of great importance in a smart-city network as users demand seamless delivery of services across various network segments such as regional data centers, wireless networks, and PONs. Smart-city applications and services lead to a traffic mix with diverse demands that require optimized resource allocation schemes across fixed and wireless converged network elements. For example, the occupants of automated shuttles rely on high-capacity broadband connectivity for entertainment and business applications, while the vehicles themselves need a latency of 1 ms or even lower and a high-bandwidth connectivity to gather information about their environment. In our work on resource allocation inside the smart-city network, we particularly focus on the PON upstream path that is often considered as the latency bottleneck because of associated waiting times for ONUs to acquire network access in a TDMA scheme. The ONUs have traffic bearing entities called transmission containers (T-CONT) that are the lowest granularity of service differentiation for bandwidth provisioning by a centralized dynamic bandwidth assignment (DBA) process in the OLT. T-CONTs can be assigned with different traffic descriptors related to bandwidth, delay properties, and prioritization. The DBA process in PONs is conceptually composed of two main components: the bandwidth assignment to each T-CONT per ONU and the bandwidth map (BWmap) generation for organizing the upstream data transport across all ONUs according to the overall bandwidth assignment [14].

In order to study the latency and bandwidth statistics, we simulated the resource allocation in a PON that provides fiber connectivity for wireless antenna sites in a fixed-wireless converged architecture. As vehicles and their wireless user entities (UEs) move inside the smart city, the UEs need to be dynamically connected and handed over from one wireless access point to another. This also implies the reconfiguration of the related wireless processing elements at the antenna site and associated optical endpoints, i.e., ONUs and T-CONTs. To enable best-in-class QoE, an efficient and proactive resource allocation for the different ONUs and T-CONTs under the dynamically changing mobility and traffic patterns is desirable. Thus, we propose to not follow the reactive measures initiated from wireless hand-overs to the PON, but to incorporate the knowledge of locomotion patterns to predict the UE mobility. From the family of process mining methods, we applied process discovery [45] to generate a Markov chain about mobility patterns. This prediction of the mobility patterns can be used to create, provision, and release T-CONTs. If a user (car) is connected to an AP and this way to an ONU (associated with the two different service classes represented by different T-CONTs), the OLT starts the creation and provisioning of T-CONTs (ONU-AP) for the most probable path from the current ONU (+AP) for the deterministic service requirement using the same BW as allocated to the current ONU T-CONT. This follows the assumptions of a constant bandwidth demand for this deterministic and time critical service. In all other

ONUs connected to APs around the currently connected AP-ONU, a handover (backoff) T-CONT was created that could be provisioned quickly if a wrong mobility path prediction were made. The pre-conditioning of the best effort traffic is assumed time uncritical and will thus follow the allocations of the remaining bandwidth of the PON link after taking into account all deterministic (assured) bandwidth of all users in the PON, the pre-provisioning, and the demand of all other users on this best effort service category. In our simulation, we consider two service types: ultra-broadband non-time critical services and medium-to-low capacity time-critical services. Furthermore, we specify three different resource allocation scenarios: (a) static initialization of the T-CONTs at each ONU, (b) full knowledge of mobility pattern and thus dynamic creation, provisioning, and release of T-CONTs, and (c) mobility pattern prediction and thus dynamic creation, provisioning, and release of T-CONTs at ONUs along the most probable paths of the vehicles (UEs). One OLT is connected to 20 ONUs and 100 vehicles (UEs) use the two service types to generate data requests for the T-CONTs at the ONUs. The path prediction of vehicles (UEs) applied in the resource allocation simulation is obtained by monitoring the connectivity of UEs to the Wi-Fi access points within the city of Karlsruhe, Germany. Event tables are generated from which transition probabilities between wireless access points and hence connected ONUs are calculated as shown in Fig. 8. The simulation reveals that the static T-CONT allocation applies a large over-subscription, which leads to a high bandwidth allocation of 110%, but allows very low latencies since the requested bandwidth is permanently available. Bandwidth allocation can be improved for broadband services to 10% and 50% and for time-critical services to 25% and 88% for the dynamic T-CONTs with known path and predicted path, respectively. For time-critical applications, the defined latency can be ensured with 0.5 ms for the known path, while it is close to the requirement with 1.4 ms for the predicted path. Broadband services even improve the latency from 7.5 ms (static T-CONT) to 6.3 ms for the known path but worsen it to 166 ms for the predicted path. The latter can be improved by further optimization of the mobility pattern prediction and therefore provide even more benefits for PON resource allocation.

5. FIBER NETWORK DEPLOYMENT

Future smart cities require densely spaced small cells, sensors, and regional data centers, all of which may become fiber endpoints. However, the exact fiber demand of such cities is still uncertain, as it is not yet clear how many of these entities will have to be placed how densely in the environment. Moreover, the financial benefits and potential revenues are intangible for today's investors and public authorities. In fact, there are few, if any, network operators that would include traffic, street lights, or road intersections as fiber endpoints in their current fiber rollout plans. At the same time, the fiber rollout to connect homes, businesses, and public buildings in Europe is gaining significant momentum. While, for instance, countries such as Germany with only 40.3% and the UK with 57% still lag behind in the fiber-to-the-home/building (FTTH/B) coverage rates, they are now among the three fastest growing FTTH markets, both in volume and percentage [46]. Since fiber deployment involves a considerable amount of work and costs, it is crucial to sustainably consider the potential future demands on the optical network.

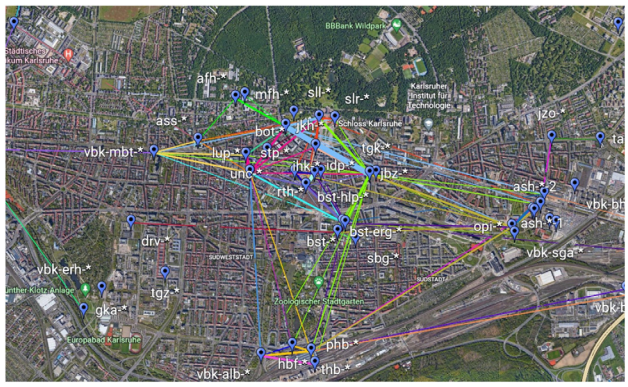

Fig. 8. Satellite image of the city of Karlsruhe, Germany. The blue pins with name codes indicate the public Wi-Fi access points in the city center. The mobility pattern of vehicles (users) accessing the access points was observed and evaluated. The transitions between the access points are represented by lines, whereby the thickness of the lines visualizes the transition probability.

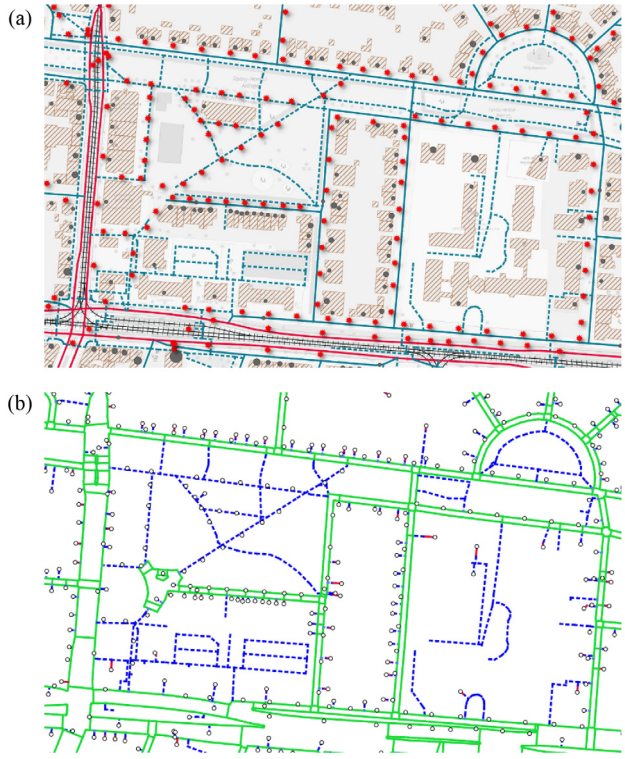

Fig. 9. From raw data to a routable base network, Karlsruhe-Weststadt. (a) Residential roads (blue), footways, paths (blue, dashed), major streets (red), railroads/tram (black), building outlines (brown), addresses (gray dots increasing in size with the number of households/businesses), and street lights (red stars). (b) Generated base network of potential routes: public street sides and potential street crossings (green), drop/private routes (blue dashed), and inhouse connections (red).

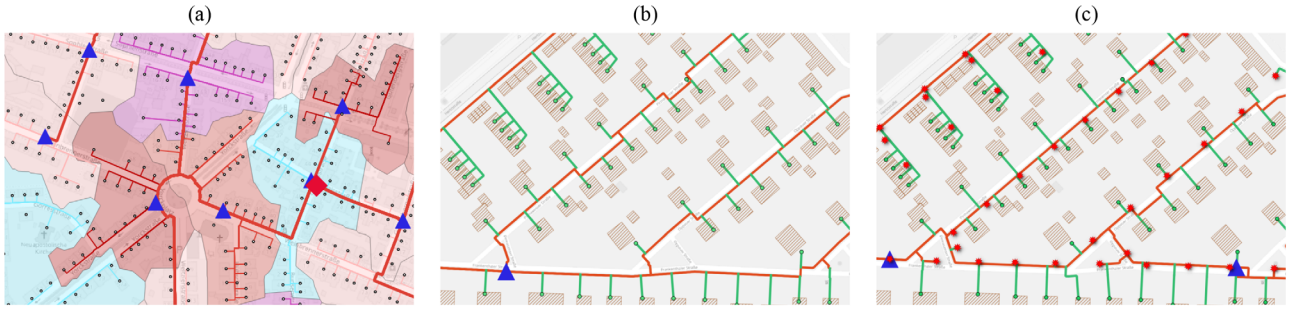

Fig. 10. Fiber access network in Karlsruhe. (a) Feeder cables (red lines) with fiber distribution points (blue triangles) connected to the central office (red diamond) and optimized distribution clusters (colored fields). (b) FTTH: the red and green lines show the routed ducts/cables for homes-passed and homes-connected paths, respectively. (c) FTTH + street light: the red stars show the street light fiber endpoints. The increased fiber demand requires an additional distribution point and slightly different routing compared to (b).

In the following, we present a techno-economic study, which shows that even a small increase in today's investments for fiber access can lead to a significant expansion of future opportunities. We optimized and compared different scenarios of fiber access networks for the western part of the city of Karlsruhe, Germany (see Figs. 9 and 10). The calculations were performed using the commercially available software application *atesio-fttx-optimizer-strategic* [47], an optimization framework to compute FTTx rollout plans, which is already in productive use at several international telecommunication operators.

The study is mainly based on public available information. We gathered data from 1700 addresses (Nexiga) in Karlsruhe, encompassing a certain number of households and business units each, the location of 500 street lights (public utility of Karlsruhe), and public infrastructure information from OpenStreetMap (OSM) [48], including streets, railroads, waterways, and building outlines.

In a first *infrastructure derivation step*, as depicted in Fig. 9, the atesio engine combines all raw data to compute a routable base network. The process entails providing two street sides starting from OSM street center-lines, introducing potential street crossings, and connecting all demand entities (addresses, street lights) with the base network. Additionally, a cost model is applied to all potential route segments, including trenching and crossing costs depending on street types, as well as railroad crossing costs, as outlined in Table 1.

In a second *optimization step*, an FTTH network is computed and embedded into the route network; see Fig. 10. We consider a greenfield scenario with typical equipment costs and a common network architecture.

That is, the distribution area is a PON, where each demand site is connected to a fiber distribution hub using 1/12/24 pipe microduct trees and 6-to-48-fiber point-to-point blown-in micro-cable routing. Each household is supposed to get one fiber, while two fibers are provided to individual business units. An address is supported with at least one cable and hence at least six fibers. The scenario with connected street lights also provides each of these sites with a 6f cable. The PON splitting hierarchy depends on the demand site. Fiber connections for addresses with up to 24 households and also street lights are split 32:1 at the fiber distribution hub. For bigger addresses with more than 24 resident units, a 4:1 splitting in the building is followed by a 8:1 splitting at the fiber distribution hub. Business units get a point-to-point connection to the central office. The fiber distribution hubs are connected in the feeder area with conventional cable trees and ducts to an optical distribution frame (ODF) at the central office (CO). The corresponding cost model is stated in Table 1 (cables, ducts, and trenching) and Table 2 (network equipment).

Table 1. Cost of Considered Connection Entities[a]

Cable cost euro/m	
Distribution 6f/12f/24f/48f	1.56/1.66/1.75/1.9
Feeder 48f/96f/192f/288f	2.72/2.84/3.5/4
Duct cost euro/m	
Distribution 1 × 6/12 × 6/24 × 6 mm	1.8/4/6.4
Feeder 4 mm × 10 mm / 7 mm × 10 mm	3/3.75
Street side trenchning cost euro/m	
Private paths, footways, tracks	60
Residential, living streets	100
Major roads (primary, secondary)	120
Street crossing cost euro/m	
Residential, living streets	100
Major roads (primary, secondary)	150
Railroad crossings cost euro/crossing	
Tram	10,000
Railway	25,000

[a]f: fiber.

The goal of the atesio engine *atesio-fttx-optimizer-strategic* is to compute a cost-optimized network. In order to achieve this objective, the software combines algorithmic intelligence and mathematical optimization solving a wide range of decision problems, from clustering (distribution areas) and routing (fibers, cables, ducts) to network design and flow problems.

The results of the study are depicted in Tables 3 and 4 for three scenarios, a pure FTTH approach connecting addresses only (FTTH), a second scenario that connects both addresses and street lights in a common PON (FTTH + Street Lights), and a third scenario that enriches the pure FTTH scenario with additional duct pipe reserves (FTTH + Reserves). Independent of the senario, the total cost of the fiber rollout is clearly dominated by trenching, accounting for 79%–80% of the homes-passed network (i.e., fiber deployment in public streets only, excluding dedicated connections to individual

Table 2. Cost in Euro of Considered Node Network Equipment

Demand sites	
House connection	100
Splitter 1:4	120
Distribution sites	
Splitter 1:8/1:32	180/250
Fiber distribution hub 48/72/96 ports	2000/3000/4100
Central office	
ODF 2500/5000 ports	25,000/30,000
Infrastructure sites	
Manhole	3000
Fiber closure	1000
Splice	10

Table 3. Cost in Euro of the Homes-Passed Share of the FTTH Network

	FTTH	FTTH + Street Lights	FTTH + Reserves
Locations	584,390	633,020	602,360
Cables	62,862	55,956	70,299
Ducts	150,348	168,836	165,272
Trenching	3,126,518	3,211,177	3,217,357
Sum	**3,924,118**	**4,068,988**	**4,055,288**

Table 4. Cost in Euro of the All-Connected FTTH Network

	FTTH	FTTH + Street Lights	FTTH + Reserves
Locations	827,430	927,820	845,420
Cables	357,984	440,616	359,100
Ducts	193,282	224,662	208,699
Trenching	4,082,661	4,370,627	4,210,922
Sum	**5,461,357**	**5,962,725**	**5,624,141**

demand sites) and 73%–75% of the full FTTH deployment (homes-connected). The homes-passed deployment takes 68%–72% of the cost, compared to the full homes-connected network. Comparing the first two scenarios, it turns out that the supplementary expense of integrating street lights along with addresses amounts to a mere 3.6% in the homes-passed cost. This might seem surprisingly small but is due to the fact that street lights in urban areas are in close vicinity to the network that is routed along the side-walks; see Figs. 9(a), 10(b), and 10(c). However, for the full FTTH deployment, incorporating street lights in addition to addresses results in a 9% cost increase due to the additional expense of last-meter excavation and exclusive point-to-point cabling. In the third scenario, the street lights have been omitted in the planning but extra pipe reserve capacity has been considered. Four out of 12 duct pipes have been kept free in the distribution area, providing 850 additional and evenly distributed reserve pipes along the homes-passed architecture. Therefore, more than 50% additional sites can be connected if the need exists without additional costs in (homes-passed) deployment. Each of these 850 pipes could accommodate a fiber cable with up to 72 fibers, ensuring a highly sustainable investment with considerable flexibility in future smart sustainable cities. Such a reserve-enriched network configuration results in a homes-passed cost increase of just 3.3%, demonstrating that explicit inclusion of highly uncertain fiber endpoints, such as street lights, is not necessary in the planning process. Instead, it suffices to provide sufficient reserves in the currently built homes-passed networks. This already greatly increases the chance of supporting future smart-city applications and means sustainable planning without over-investment.

6. REMOTE ASSISTANCE

Autonomous vehicles will occasionally require human support in challenging situations, such as traffic accidents, emergency scenarios, or construction zones, as explained in Fig. 1. Remote assistance for autonomous driving in emulated traffic situations has been successfully demonstrated as a use case for smart cities in the KIGLIS project [49]. The demonstration setup for remote monitoring and assistance of an autonomous vehicle using a PON-based point-to-multipoint system is shown in Fig. 11. In this demonstration, we employ a XGS-PON OLT in the control center and XGS-PON ONUs in the remote node. In this field demonstration setup, the XGS-PON ONUs are connected to different wireless network infrastructures and the EDGE cloud. The intelligent infrastructure consists of various surveillance systems and sensors. The communication infrastructure employs public radio frequencies, such as WiFi technology, to communicate with the autonomous vehicle. A picture of the control center and the fully connected autonomous vehicle is shown at the bottom of Fig. 11. A prerequisite for the remote assistance is the transmission of high volumes of sensor data from the fully connected autonomous vehicle over the PON infrastructure and, if applicable, from the infrastructure sensors as well. In order to ensure real-time transmission in a future smart city, which will have a high number of connected units and thus high communication traffic, we have investigated and developed various methods dedicated to autonomous driving. This includes AI-based compression methods for lidar and camera data.

In [50], the project explored the use of deep generative neural networks for compressing sensor data, achieving better reconstruction quality compared to traditional methods such as JPEG. Specifically, variational autoencoders (VAEs) and generative adversarial networks (GANs) were utilized to compress both lidar and image data, ensuring efficient data transmission without overloading the network infrastructure. The implemented compression methods demonstrated promising results in maintaining the data integrity and quality necessary for remote assistance. In combination with the network infrastructure, it was possible to give a successful demonstration of the explored methods in the Test Area Autonomous Driving Baden-Württemberg (TAF-BW). The integration of cooperative perception, involving data from multiple sources such as infrastructure sensors and other vehicles, proved to enhance the overall reliability and efficiency of the remote assistance system.

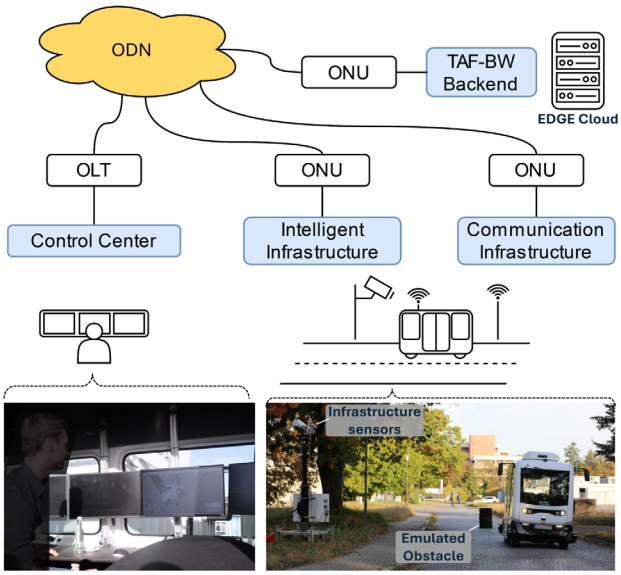

Fig. 11. Demonstration setup of the remote assistance of an autonomous vehicle by a remote control center as a typical smart-city use case.

During the field test, the setup involved an autonomous shuttle operating within the TAF-BW, a semi-private test area equipped with various infrastructural sensors. The simulated problem scenario involved placing a static obstacle in the path of the autonomous vehicle, requiring it to switch from autonomous mode to remote assistance mode to navigate around the obstacle safely; see Fig. 11. The remote operator, situated in a control center, used the real-time data transmitted through a PON from the vehicle's sensors and additional cooperative perception inputs to guide the vehicle around the obstacle. This setup allows us to demonstrate the capability for event detection and remote monitoring over a live optical network for an autonomous traffic system.

Additionally, the scalable remote operation system outlined in [49] was utilized during the field test. This system, which integrates cooperative perception and open-source communication modules, ensures robust and efficient data exchange between the autonomous vehicle, control center, and external sensors. The communication system is based on the robot operating system (ROS) and utilizes a Docker container for ease of deployment and maintenance, ensuring scalable and adaptable communication across various network configurations.

In conclusion, we showcased the practical viability of remote assistance for autonomous vehicles, highlighting the importance of advanced data compression techniques and cooperative perception in maintaining robust and efficient remote operation systems.

7. CONCLUSION

Emerging smart-city applications, such as connected driving, place stringent demands on the optical-access network. We demonstrate that a 100-Gbit/s IM/DD and 200-Gbit/s coherent PON can fulfill these requirements. Furthermore, we demonstrate that OTDR measurements can be augmented with ML techniques to classify OTDR events. In future efforts, more efficient artificial intelligence methods can be used to exploit these results for network failure prediction. We have simulated that DBA, taking into account the mobility behavior of traffic participants, can increase the efficiency of bandwidth allocation and guarantee low latency. Moreover, our cost study on fiber deployment in the German city of Karlsruhe provides impetus for a sustainable fiber rollout that will also meet the future needs of our cities. Finally, we demonstrate in a field test remote operation of a fully connected vehicle to steer the shuttle around an obstacle in real time. The comprehensive work from fiber-access infrastructure to fiber deployment and real-world application within the KIGLIS project provides technical achievements and valuable insights on the way to a fully connected smart and sustainable city of the future.

Funding. Bundesministerium für Bildung und Forschung (16KIS1228, 16KIS1227K, 16KIS1230, 16KIS1232, 16KIS1233, 16KIS1231, 16KISK010).

Acknowledgment. The authors thank Abderrahim Ramdane from CNRS, Paris, for providing the MLLD chip and Ute Troppenz from Fraunhofer Institute HHI, Berlin, for providing the DFB laser chips.

Disclosures. The authors declare no conflicts of interest.

REFERENCES

1. ITU, "IMT traffic estimates for the years 2020 to 2030," Report ITU-R M.2370-0 (2015).
2. W. Jiang, B. Han, M. A. Habibi, *et al.*, "The road towards 6G: a comprehensive survey," IEEE Open J. Commun. Soc. **2**, 334–366 (2021).
3. R. Bonk, "The future of passive optical networks," in *International Conference on Optical Network Design and Modeling (ONDM)* (IEEE, 2021).
4. D. Bogdoll, P. Matalla, C. Füllner, *et al.*, "KIGLIS: smart networks for smart cities," in *IEEE International Smart Cities Conference (ISC2)* (IEEE, 2021).
5. "Artificial Intelligence for the Optimization of Fiber Optic Networks in a Smart City, in German: Künstliche Intelligenz zur Optimierung von Glasfasernetzen in einer intelligenten Stadt," 2020, https://www.forschung-it-sicherheit-kommunikationssysteme.de/projekte/kiglis.
6. ITU, "Smart sustainable cities: an analysis of definitions," ITU-T, FG-SSC (2015).
7. B. N. Silva, M. Khan, and K. Han, "Towards sustainable smart cities: a review of trends, architectures, components, and open challenges in smart cities," Sustain. Cities Soc. **38**, 697–713 (2018).
8. P. J. Basford, F. M. J. Bulot, M. Apetroaie-Cristea, *et al.*, "LoRaWAN for smart city IoT deployments: a long term evaluation," Sensors **20**, 648 (2020).
9. J. Maes, S. Bidkar, M. Straub, *et al.*, "Efficient transport of enhanced CPRI fronthaul over PON [Invited]," J. Opt. Commun. Netw. **16**, A136–A142 (2024).
10. S. Bidkar, T. Kale, J. Ho, *et al.*, "Demonstration of cooperative transport interface enabled cooperative DBA for 5G fronthaul over TDM-PON," in *European Conference on Optical Communication (ECOC)* (2023), pp. 503–506.
11. E. Harstead, "25G based PON technology," in *Optical Fiber Communication Conference (OFC)* (Optica Publishing Group, 2018), paper Tu2B.5.
12. 25GS-PON, "25GS-PON specification-version 3.0," Multi-source agreement (2023).
13. ITU, "50-gigabit-capable passive optical networks (50G-PON): physical media dependent (PMD) layer specification," ITU-T Recommendation G.9804.3 (2021).
14. T. Pfeiffer, P. Dom, S. Bidkar, *et al.*, "PON going beyond FTTH [Invited Tutorial]," J. Opt. Commun. Netw. **14**, A31–A40 (2022).

15. V. Houtsma and D. van Veen, "Reusing data center optics and solutions for beyond 25 Gb/s PON: is the gap really bridged?" in *Optical Fiber Communication Conference (OFC)* (2023), paper W1I.1.
16. P. Torres-Ferrera, F. Effenberger, M. S. Faruk, *et al.*, "Overview of high-speed TDM-PON beyond 50 Gbps per wavelength using digital signal processing [Invited Tutorial]," J. Opt. Commun. Netw. **14**, 982–996 (2022).
17. R. Borkowski, Y. Lefevre, A. Mahadevan, *et al.*, "FLCS-PON—an opportunistic 100 Gbit/s flexible PON prototype with probabilistic shaping and soft-input FEC: operator trial and ODN case studies," J. Opt. Commun. Netw. **14**, C82–C91 (2022).
18. N. Dubrovina, E. Durán-Valdeiglesias, H. Debrégeas, *et al.*, "Record high power 13 dBm electro-absorption modulated laser for 50G-PON," in *European Conference on Optical Communication (ECOC)* (IEEE, 2022), paper Th1E.6.
19. VPIphotonics GmbH, https://www.vpiphotonics.com.
20. B. Smith, I. Lyubomirsky, and S. Bhoja, "Leveraging 400G ZR FEC technology," in *IEEE 802.3 Beyond 10 km Optical PHYs Study Group* (2017).
21. V. Lauinger, P. Matalla, J. Ney, *et al.*, "Fully-blind neural network based equalization for severe nonlinear distortions in 112 Gbit/s passive optical networks," in *Optical Fiber Communication Conference (OFC)* (2024), paper Th3J.5.
22. C. Shao, E. Giacoumidis, S. Li, *et al.*, "A novel machine learning-based equalizer for a downstream 100G PAM-4 PON," in *Optical Fiber Communication Conference (OFC)* (2024), paper W1H.1.
23. C. Shao, E. Giacoumidis, P. Matalla, *et al.*, "Advanced equalization in 112 Gb/s upstream PON using a novel Fourier convolution-based network," in *European Conference on Optical Communication (ECOC)* (2024), paper W3D.2.
24. R. Fischer, P. Matalla, S. Randel, *et al.*, "Non-linear equalization in 112 Gb/s PONs using Kolmogorov-Arnold networks," arXiv (2024).
25. S. Miladić-Tešić, G. Marković, D. Peraković, *et al.*, "A review of optical networking technologies supporting 5G communication infrastructure," Wirel. Netw. **28**, 459–467 (2022).
26. P. Matalla, M. S. Mahmud, C. Füllner, *et al.*, "Real-time feedforward clock recovery for optical burst-mode transmission," in *Optical Fiber Communication Conference (OFC)* (2022), paper M2H.2.
27. P. Matalla, C. Koos, and S. Randel, "Comparison of feedback and feedforward clock recoveries for ultra-fast synchronization in passive optical networks," in *Optical Fiber Communication Conference (OFC)* (2024), paper W2A.36.
28. J. Zhang and Z. Jia, "Coherent passive optical networks for 100G/1- and-beyond fiber access: recent progress and outlook," IEEE Netw. **36**, 116–123 (2022).
29. A. Hraghi, G. Rizzelli, A. Pagano, *et al.*, "Analysis and experiments on C band 200G coherent PON based on Alamouti polarization-insensitive receivers," Opt. Express **30**, 46782–46797 (2022).
30. I. B. Kovacs, M. S. Faruk, and S. J. Savory, "A minimal coherent receiver for 200 Gb/s/1 PON downstream with measured 29 dB power budget," IEEE Photonics Technol. Lett. **35**, 257–260 (2023).
31. H. Rohde, E. Gottwald, S. Rosner, *et al.*, "Trials of a coherent UDWDM PON over field-deployed fiber: real-time LTE backhauling, legacy and 100G coexistence," J. Lightwave Technol. **33**, 1644–1649 (2015).
32. A. Rashidinejad, A. Yekani, T. A. Eriksson, *et al.*, "Real-time point-to-multipoint for coherent optical broadcast and aggregation–enabled by digital subcarrier multiplexing," in *Optical Fiber Communication Conference (OFC)* (2023), paper W3H.1.
33. J. Zhang, Z. Jia, H. Zhang, *et al.*, "Rate-flexible single-wavelength TFDM 100G coherent PON based on digital subcarrier multiplexing technology," in *Optical Fiber Communication Conference (OFC)* (2020), paper W1E.5.
34. Z. Xing, K. Zhang, X. Chen, *et al.*, "First real-time demonstration of 200G TFDMA coherent PON using ultra-simple ONUs," in *Optical Fiber Communication Conference (OFC)* (2023), paper Th4C.4.
35. R. Gaudino, V. Curri, G. Bosco, *et al.*, "On the use of DFB lasers for coherent PON," in *Optical Fiber Communication Conference (OFC)* (2012), paper OTh4G.1.
36. G. Yoffe, S. Zou, S. Rishton, *et al.*, "Widely-tunable 30mw laser source with sub-500khz linewidth using DFB array," in *21st Annual Meeting of the IEEE Lasers and Electro-Optics Society (LEOS)* (2008), pp. 892–893.
37. M. M. H. Adib, C. Füllner, J. N. Kemal, *et al.*, "Colorless coherent TDM-PON based on a frequency-comb laser," J. Lightwave Technol. **40**, 4287–4299 (2022).
38. J. Zhang, G. Li, S. Xing, *et al.*, "Flexible and adaptive coherent PON for next-generation optical access network," Opt. Fiber Technol. **75**, 103190 (2023).
39. J. Zhou, Z. Xing, H. Wang, *et al.*, "Flexible coherent optical access: architectures, algorithms, and demonstrations," J. Lightwave Technol. **42**, 1193–1202 (2024).
40. R. Borkowski, M. Straub, Y. Ou, *et al.*, "FLCS-PON—a 100 Gbit/s flexible passive optical network: concepts and field trial," J. Lightwave Technol. **39**, 5314–5324 (2021).
41. M. M. H. Adib, C. Füllner, H. Peng, *et al.*, "Coherent time- and wavelength-division multiplexed point-to-multipoint optical access network using low-cost DFB lasers enabled by a frequency comb," Opt. Express **32**, 38516–38530 (2024).
42. M. M. H. Adib, C. Füllner, C. Koos, *et al.*, "Subcarrier-based coherent PON architecture for a converged fiber infrastructure in smart cities," in *Optica Advanced Photonics Congress* (Optica Publishing Group, 2022), paper NeM3D.2.
43. T. Hastie, R. Tibshirani, J. Friedman, *et al.*, "Random forests," in *The Elements of Statistical Learning: Data Mining, Inference, and Prediction* (2009), pp. 587–604.
44. M. Straub, J. Reber, T. Saier, *et al.*, "ML approaches for OTDR diagnoses in passive optical networks—event detection and classification: ways for ODN branch assignment," J. Opt. Commun. Netw. **16**, C43–C50 (2024).
45. W. M. P. van der Aalst, *Foundations of Process Discovery* (Springer International Publishing, 2022), pp. 37–75.
46. FTTH Council Europe, "European FTTH/B market panorama 2024," (September 2023).
47. atesio GmbH, http://www.atesio.de.
48. OpenStreetMap, https://www.openstreetmap.org.
49. M. Gontscharow, J. Doll, A. Schotschneider, *et al.*, "Scalable remote operation for autonomous vehicles: integration of cooperative perception and open source communication," in *IEEE Intelligent Vehicles Symposium (IV)* (2024), pp. 43–50.
50. D. Bogdoll, J. Jestram, J. Rauch, *et al.*, "Compressing sensor data for remote assistance of autonomous vehicles using deep generative models," in *Conference on Neural Information Processing Systems Workshop on Machine Learning for Autonomous Driving (NeurIPS)* (2021), paper ML4AD.